

Two new hetero-dinuclear nickel(II)/zinc(II) complexes with compartmental Schiff bases: Synthesis, characterization and self assembly



Anik Bhattacharyya, Sourav Roy, Jhonti Chakraborty, Shouvik Chattopadhyay*

Department of Chemistry, Inorganic Section, Jadavpur University, Kolkata 700032, India

ARTICLE INFO

Article history:

Received 12 February 2016

Accepted 15 March 2016

Available online 26 April 2016

Keywords:

Zinc(II)

Nickel(II)

Hetero-dinuclear

Compartmental Schiff base

Photoluminescence

ABSTRACT

Two compartmental Schiff bases, H_2L^1 [N,N'-bis(3-methoxysalicylidene)propane-1,3-diamine] and H_2L^2 [N,N'-bis(3-methoxysalicylidene)-2,2-dimethylpropane-1,3-diamine], have been utilized to prepare two hetero-dinuclear nickel(II)/zinc(II) complexes, $[(DMSO)_2NiL^1Zn(NCS)_2]$ (**1**) and $[(DMSO)_2NiL^2Zn(NCS)_2]$ (**2**). Both complexes have been characterized by elemental and spectral analysis. Single crystal X-ray diffraction analysis has confirmed their structures. The key step in the synthesis of these complexes is to use nickel(II) thiocyanate tetrahydrate and zinc(II) acetate dihydrate in a single pot. In each complex, octahedral nickel(II) is placed in the inner N_2O_2 compartment (with DMSO molecules being coordinated in the axial sites) and tetrahedral zinc(II) is placed in the outer O_4 compartment of the Schiff bases. Supramolecular interactions in both complexes were explored. Both complexes show photoluminescence in DMSO solution at room temperature upon the irradiation of ultraviolet light. The life times of the excited states are in the range of 4–5 ns.

© 2016 Elsevier Ltd. All rights reserved.

1. Introduction

Synthesis and characterization of di and polynuclear 3d metal complexes have attracted the attentions of material scientist since long for their potential uses in non-linear optics, biological modeling application, magnetism, catalysis, opto-electronic devices, molecular architectures etc [1–6]. Nickel(II) have been extensively used in preparing such complexes probably because its flexibility in attending varieties of geometries viz. square planar, square pyramidal, trigonal bipyramidal, octahedral etc with coordination numbers ranging from 4 to 6 [7–10]. On the other hand, zinc is the second most abundant 3d metal in the human body and is an essential cofactor in many biological processes [11,12]. Zinc(II) with d^{10} electronic configuration may also adopt varieties of geometries with no CFSE in any geometry [13,14].

Synthetic inorganic chemists have prepared varieties of di and polynuclear transition metal complexes with well-known salen type Schiff base ligands utilizing the bridging ability of their phenoxy oxygen atoms [15,16]. Salen type ligands prepared using 3-methoxysalicylaldehyde instead of salicylaldehyde itself is more advantageous because they have inner N_2O_2 and outer O_4 cores and may be considered as compartmental Schiff bases

[17–20]. Several homo and hetero-di and polynuclear transition and non-transition metal complexes have been prepared with these ligands [21–24]. Many 3d/4f complexes with these compartmental ligands have been found to show ferromagnetic properties [25,26]. However, phenoxo bridged hetero-dinuclear zinc(II)/nickel(II) complexes did not receive such high attention probably because of the lack of magnetic exchange interaction in them. In this context, it is noteworthy that the importance of the d^{10} metal complexes lies in their strong luminescence properties and potential applications in electronic and optoelectronic devices [27,28].

In the present work, we have used two compartmental Schiff bases to prepare two hetero-dinuclear nickel(II)/zinc(II) complexes with NiO_2Zn cores. These are the first examples of any hetero-dinuclear nickel(II)/zinc(II) complexes with salen type Schiff bases. Both complexes exhibit photoluminescence in DMSO medium with lifetime 4–5 ns. Herein, we would like to report the synthesis, characterization, X-ray crystal structure and supramolecular architecture of two new hetero-dinuclear nickel(II)/zinc(II) complexes.

2. Experimental

Nickel(II) thiocyanate tetrahydrate was prepared in laboratory following the literature method [29]. All other materials were commercially available, reagent grade and used as purchased from Sigma-Aldrich without further purification.

* Corresponding author. Tel.: +91 33 2457 2941.

E-mail address: shouvik.chem@gmail.com (S. Chattopadhyay).

2.1. Synthesis

2.1.1. Synthesis of ligands

2.1.1.1. Synthesis of H_2L^1 [*N,N'*-bis(3-methoxysalicylidene)propane-1,3-diamine]. A methanol solution (10 ml) of 3-methoxysalicylaldehyde (304 mg, 2 mmol) and 1,3-diaminopropane (0.13 ml, 1 mmol) was refluxed for ca. 1 h. The ligand was not isolated and used directly for the synthesis of the complex **1**.

2.1.1.2. Synthesis of H_2L^2 [*N,N'*-bis(3-methoxysalicylidene)-2,2-dimethylpropane-1,3-diamine]. It was prepared in a similar method as that of H_2L^1 except that 2,2-dimethyl-1,3-diaminopropane (0.12 ml, 1 mmol) was used instead of 1,3-diaminopropane. The ligand was not isolated and used directly for the synthesis of the complex **2**.

2.1.2. Synthesis of complexes

2.1.2.1. Synthesis of $[(DMSO)_2NiL^1Zn(NCS)_2]$ (1**).** A methanol (10 ml) solution of zinc(II) acetate dihydrate (219 mg, 1 mmol) was added to the methanol solution (20 ml) of H_2L^1 and the resulting solution was stirred for 15 min. A methanol (10 ml) solution of nickel(II) thiocyanate tetrahydrate (250 mg, 1 mmol) was then added to it. The stirring was continued for about 2 h. Few drops of DMSO was added and the resulting solution was kept for crystallization. Single crystals, suitable for X-ray diffraction, were obtained after 3–4 days on slow evaporation of the solution in open atmosphere.

Yield: 552 mg, 75%. *Anal. Calc.* for $C_{25}H_{32}N_4NiO_6S_4Zn$ (FW = 736.87): C, 40.75; H, 4.38; N, 7.60. Found: C, 40.8; H, 4.2; N, 7.7%. FT-IR (KBr, cm^{-1}): 1626 (C=N); 2074 (NCS). UV-Vis [λ_{max} (nm)] [ϵ_{max} ($L mol^{-1} cm^{-1}$)] (DMSO): 280 (2.96×10^4); 352 (2.71×10^4); 580 (8.75); 993 (6.79). Magnetic moment = 3.13 BM.

2.1.2.2. Synthesis of $[(DMSO)_2NiL^2Zn(NCS)_2]$ (2**).** It was prepared in a similar method as that of complex **1** except that H_2L^2 was used instead of H_2L^1 . Single crystals, suitable for X-ray diffraction, were obtained after 3–4 days on slow evaporation of the solution in open atmosphere.

Yield: 596 mg, 78%. *Anal. Calc.* for $C_{27}H_{36}N_4NiO_6S_4Zn$ (FW = 764.92): C, 42.39; H, 4.74; N, 7.32. Found: C, 42.4; H, 4.6; N, 7.4%. FT-IR (KBr, cm^{-1}): 1626 (C=N); 2088 (NCS). UV-Vis [λ_{max} (nm)] [ϵ_{max} ($L mol^{-1} cm^{-1}$)] (DMSO): 290 (3.16×10^4); 363 (3.43×10^4); 577 (9.87); 987 (5.75). Magnetic moment = 3.11 BM.

2.2. Physical measurements

Elemental analyses (carbon, hydrogen and nitrogen) were performed using a Perkin Elmer 240C elemental analyzer. IR spectra in KBr ($4500\text{--}500\text{ cm}^{-1}$) were recorded with a Perkin Elmer Spectrum Two spectrophotometer. Electronic spectra in DMSO were recorded on a Perkin Elmer Lambda 35 UV-Vis spectrophotometer. Steady state photoluminescence spectra in DMSO were obtained in Shimadzu RF-5301PC spectrofluorometer at room temperature. Time dependent photoluminescence spectra were recorded using Hamamatsu MCP photomultiplier (R3809) and were analyzed by using IBHDAS6 software. The emissions of complexes are tentatively attributed to the intra-ligand transitions modified by metal coordination. Intensity decay profiles were fitted to the sum of exponentials series $I(t) = \sum_i \alpha_i \exp\left(-\frac{t}{\tau_i}\right)$, where α_i was a factor representing the fractional contribution to the time resolved decay of the component with a lifetime of τ_i . Bi-exponential function was used to fit the decay profile for both complexes, with obtaining χ^2 close to 1. The intensity-averaged life time (τ_{av}) was determined from the result of the exponential model using $\tau_{av} = \frac{\sum_i \alpha_i \tau_i^2}{\sum_i \alpha_i \tau_i}$, where α_i and τ_i are the pre-exponential factors and excited state

Table 1

Crystal data and refinement details of complexes **1** and **2**.

Complex	1	2
Formula	$C_{25}H_{32}N_4NiO_6S_4Zn$	$C_{27}H_{36}N_4NiO_6S_4Zn$
Formula weight	736.91	764.96
T (K)	100	100
Crystal system	triclinic	triclinic
Space group	$P\bar{1}$	$P\bar{1}$
a (Å)	12.6431(4)	10.1450(3)
b (Å)	15.8433(5)	11.1743(3)
c (Å)	16.0431(5)	16.8051(4)
α (°)	85.146(2)	74.984(1)
β (°)	89.705(2)	74.933(1)
γ (°)	87.339(2)	74.006(1)
Z	4	2
D_{calc} ($g\text{ cm}^{-3}$)	1.530	1.467
μ (mm^{-1})	1.643	1.520
F(000)	1520	792
Total reflections	48633	26483
Unique reflections	12564	6634
Observed data [$I > 2\sigma(I)$]	9195	4692
No. of parameters	739	398
R_{int}	0.052	0.032
R_1, wR_2 (all data)	0.0634, 0.1100	0.0781, 0.1538
R_1, wR_2 [$I > 2\sigma(I)$]	0.0418, 0.0998	0.0544, 0.1399

Table 2

Selected bond lengths (Å) for complexes **1** (subunit A) and **2**.

Complex	1	2
Zn(1)–O(1)	2.027(2)	2.056(3)
Zn(1)–O(2)	2.020(2)	2.015(3)
Zn(1)–N(3)	1.947(3)	1.957(5)
Zn(1)–N(4)	1.955(3)	1.936(5)
Ni(1)–O(1)	2.029(2)	2.020(3)
Ni(1)–O(2)	2.014(2)	1.992(3)
Ni(1)–O(5)	2.123(2)	2.106(4)
Ni(1)–O(6)	2.159(2)	2.134(3)
Ni(1)–N(1)	2.030(3)	2.010(4)
Ni(1)–N(2)	2.027(3)	2.011(3)

Table 3

Selected bond angles (°) for complexes **1** (subunit A) and **2**.

Complex	1	2
O(1)–Zn(1)–O(2)	79.13(9)	77.01(12)
O(1)–Zn(1)–N(3)	115.39(12)	106.86(16)
O(1)–Zn(1)–N(4)	112.79(12)	118.68(16)
O(2)–Zn(1)–N(3)	111.69(12)	118.03(18)
O(2)–Zn(1)–N(4)	117.81(12)	108.89(17)
N(3)–Zn(1)–N(4)	115.18(13)	120.05(19)
O(1)–Ni(1)–O(2)	79.21(9)	78.36(12)
O(1)–Ni(1)–O(5)	88.65(9)	87.99(13)
O(1)–Ni(1)–O(6)	90.46(9)	94.84(12)
O(1)–Ni(1)–N(1)	91.14(10)	91.62(14)
O(1)–Ni(1)–N(2)	168.98(10)	171.11(12)
O(2)–Ni(1)–O(5)	90.18(10)	92.21(13)
O(2)–Ni(1)–O(6)	87.04(9)	89.73(12)
O(2)–Ni(1)–N(1)	168.81(11)	169.83(14)
O(2)–Ni(1)–N(2)	91.36(9)	92.96(13)
O(5)–Ni(1)–O(6)	177.19(9)	176.85(13)
O(5)–Ni(1)–N(1)	95.29(11)	89.12(14)
O(5)–Ni(1)–N(2)	85.66(10)	90.49(14)
O(6)–Ni(1)–N(1)	87.39(11)	89.42(13)
O(6)–Ni(1)–N(2)	94.77(10)	86.93(13)
N(1)–Ni(1)–N(2)	98.77(11)	97.12(14)

luminescence decay time associated with the *i*-th component, respectively. The magnetic susceptibility measurements were performed with an EG and PAR vibrating sample magnetometer, model 155 at room temperature (300 K) in a 5000 G magnetic field, and diamagnetic corrections were performed using Pascal's

Table 4

Geometric features (distances in Å and angles in °) of the C–H... π interactions obtained for complexes **1** and **2**.

Complex	C–H...Cg(Ring)	H...Cg (Å)	C–H...Cg (°)	C...Cg (Å)
1	C(23)–H(23A)...Cg(7) ^a	2.68	136	3.433(4)
	C(24)–H(24A)...Cg(15) ^b	2.92	146	3.749(4)
	C(25)–H(25A)...Cg(8) ^b	2.84	135	3.583(4)
	C(29)–H(29)...Cg(7) ^b	2.95	150	3.787(4)
	C(47)–H(47A)...Cg(15) ^c	2.97	133	3.690(5)
2	C(22)–H(22A)...Cg(8) ^d	2.71	143	3.523(7)

Symmetry transformations: ^a = 2 – x, –y, 1 – z; ^b = 2 – x, 1 – y, 1 – z; ^c = 3 – x, 1 – y, 2 – z; ^d = 1 – x, 1 – y, –z.

Cg(7) = Centre of gravity of the ring [C(2)–C(3)–C(4)–C(5)–C(6)–C(7)]; Cg(8) = Centre of gravity of the ring [C(13)–C(14)–C(15)–C(16)–C(17)–C(18)]; Cg(15) = Centre of gravity of the ring [C(27)–C(28)–C(29)–C(30)–C(31)–C(32)] for complex **1** and Cg(8) = Centre of gravity of the ring [C(15)–C(16)–C(17)–C(18)–C(19)–C(20)] for complex **2**.

constants. Effective magnetic moments were calculated using the formula $\mu_{\text{eff}} = 2.828(\chi_{\text{MT}})^{1/2}$, where χ_{M} is the corrected molar susceptibility. The instrument was calibrated using metallic nickel. Powder X-ray diffraction were performed on a Bruker D8 instrument with Cu K α radiation. In this process, the complexes were ground with a mortar and pestle to prepare fine powders. The powders were then dispersed with alcohol onto a zero background holder (ZBH). The alcohol was allowed to evaporate to provide a nice, even coating of powder adhered to the sample holder.

2.3. X-ray crystallography

Suitable single crystals of complexes **1** and **2** were used for data collection using a 'Bruker SMART APEX II' diffractometer equipped with graphite-monochromated Mo K α radiation ($\lambda = 0.71073$ Å) at 100 K. The molecular structures were solved by direct method and refined by full-matrix least squares on F^2 using the SHELX-2014 package [30,31]. Non-hydrogen atoms were refined with anisotropic thermal parameters. The hydrogen atoms were placed in their geometrically idealized positions and constrained to ride on their parent atoms. Multi-scan empirical absorption corrections were

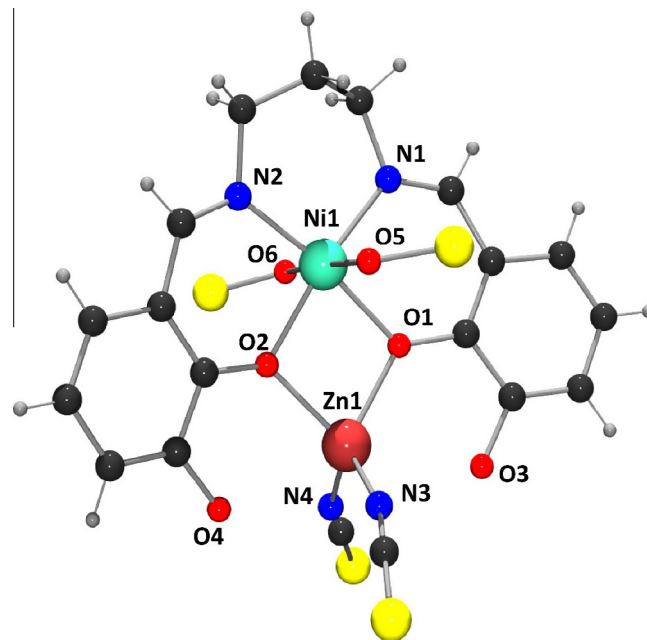
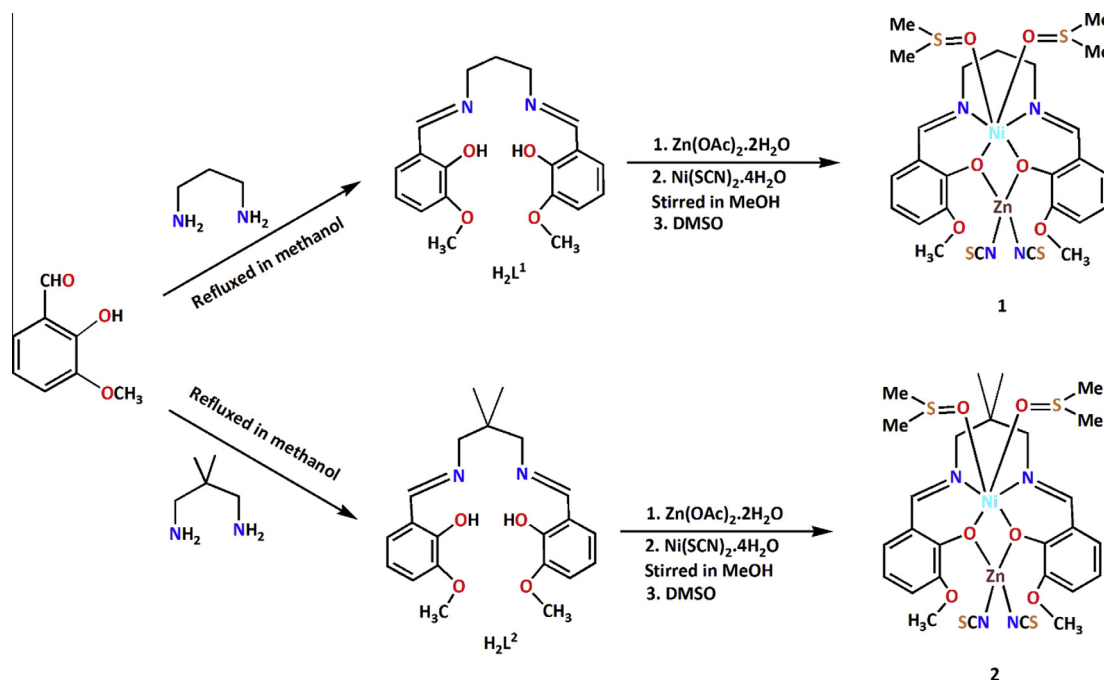


Fig. 1. Perspective view of complex **1** (subunit A) with selective atom numbering scheme. Methyl groups have been omitted for clarity.

applied to the data using the program SADABS [32]. Details of crystallographic data and refinement details are given in Table 1. Important bond lengths and angles are listed in Tables 2–5 respectively.

2.4. Hirshfeld surfaces

Hirshfeld surfaces [33–35] and the associated 2D-fingerprint [36–38] plots were calculated using Crystal Explorer [39] which accepted a structure input file in CIF format. Bond lengths to hydrogen atoms were set to standard values. For each point on



Scheme 1. Synthetic route to ligands and complexes.

the Hirshfeld isosurface, two distances d_e , the distance from the point to the nearest nucleus external to the surface and d_i , the distance to the nearest nucleus internal to the surface, were defined. The normalized contact distance (d_{norm}) based on d_e and d_i was given by

$$d_{\text{norm}} = \frac{(d_i - r_i^{\text{vdw}})}{r_i^{\text{vdw}}} + \frac{(d_e - r_e^{\text{vdw}})}{r_e^{\text{vdw}}}$$

where r_i^{vdw} and r_e^{vdw} were the van der Waals radii of the atoms. The value of d_{norm} was negative or positive depending on intermolecular contacts, being shorter or longer than the van der Waals separations. The parameter d_{norm} displayed a surface with a red-white-blue color scheme, where bright red spots highlighted shorter contacts, white areas represented contacts around the van der Waals separation, and blue regions were devoid of close contacts. For a given crystal structure and set of spherical atomic electron densities, the Hirshfeld surface was unique [40] and it was this property that suggested the possibility of gaining additional insight into the intermolecular interaction of molecular crystals.

3. Results and discussion

3.1. Synthesis

3-Methoxysalicylaldehyde has been refluxed with 1,3-diaminopropane and 2,2-dimethyl-1,3-diaminopropane respectively to form two compartmental Schiff base ligands, H_2L^1 and H_2L^2 , respectively following the literature method [17,19,21,22]. These Schiff bases on reaction with zinc(II) acetate dihydrate and nickel(II) thiocyanate tetrahydrate give two hetero-dinuclear complexes. Formation of both complexes is shown in Scheme 1. Addition of only nickel(II) thiocyanate tetrahydrate (1 mmol) produced mononuclear complexes $[(\text{H}_2\text{O})_2\text{NiL}^1]$ and $[\text{NiL}^2] \cdot 1.75\text{H}_2\text{O}$, structures of which were already reported by other groups [41–43]. The effort to convert these complexes into complexes **1** and **2** by dissolving them in DMSO followed by adding with zinc(II) acetate dihydrate and sodium thiocyanate was not successful. The key step in the synthesis of these complexes is to use nickel(II) thiocyanate tetrahydrate and zinc(II) acetate dihydrate in a single pot.

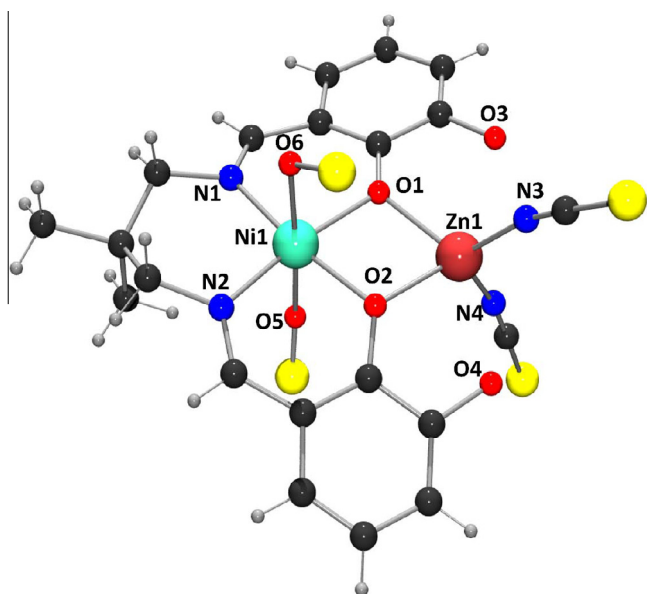


Fig. 2. Perspective view of complex **2** with selective atom numbering scheme. Methyl groups attached to oxygen and sulfur atoms have been omitted for clarity.

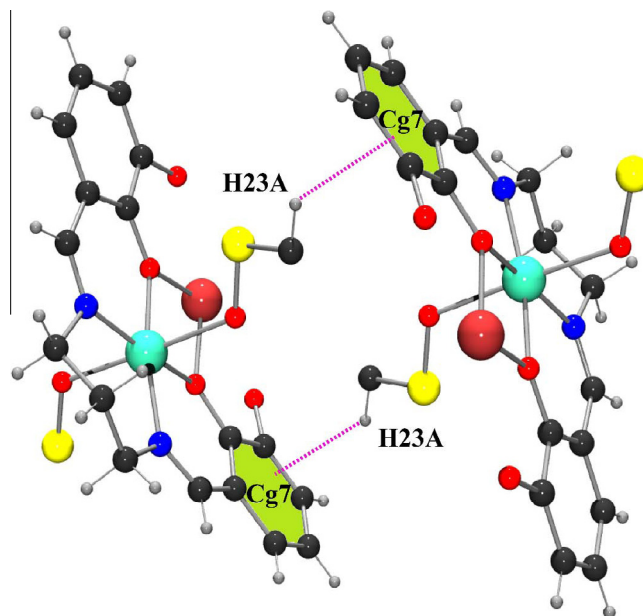


Fig. 3. Perspective view of a supra-molecular dimer formed by inter-molecular C-H... π interactions of complex **1** with selective atom numbering scheme. Only relevant atoms are shown in the figure.

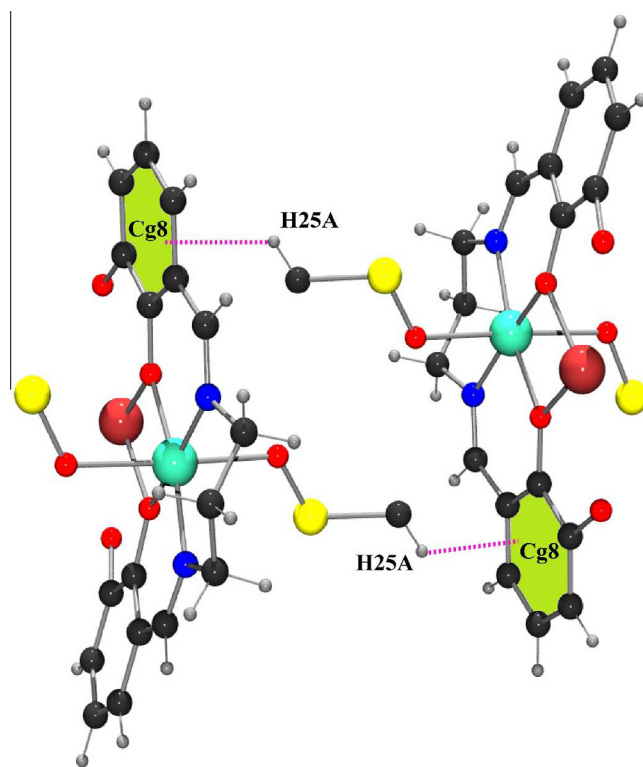


Fig. 4. Perspective view of a supra-molecular dimer formed by inter-molecular C-H... π interactions of complex **1** with selective atom numbering scheme. Only relevant atoms are shown in the figure.

3.2. Structure description

3.2.1. $[(\text{DMSO})_2\text{NiL}^1\text{Zn}(\text{NCS})_2]$ (**1**) and $[(\text{DMSO})_2\text{NiL}^2\text{Zn}(\text{NCS})_2]$ (**2**)

Complex **1** and **2** both crystallize in the triclinic space group $P\bar{1}$. The X-ray crystal structure determination reveals that in complex **1** there are two independent dinuclear subunits (A and B) with

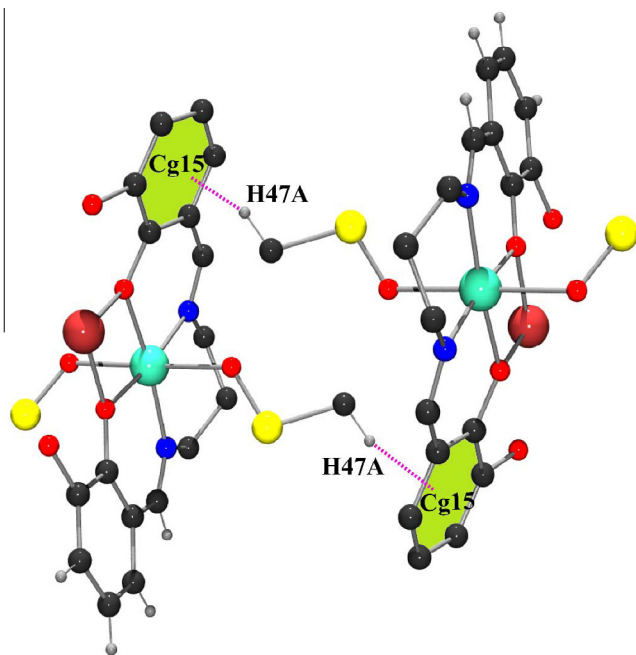


Fig. 5. Perspective view of the supra-molecular dimer formed by inter-molecular C–H $\cdots\pi$ interactions of complex **1** with selective atom numbering scheme. Only relevant atoms are shown in the figure.

equivalent geometry. Perspective views of complex **1** (subunit A) and complex **2** are given in Figs. 1 and 2 respectively. Selected bond lengths and bond angles are listed in Tables 2 and 3. The structures of subunit A of complex **1** along with that of complex **2** are described in the following paragraphs. The perspective view and description of the structure of subunit B with selective atom numbering scheme of complex **1** is given in the [Supplementary information \(SI\)](#).

The molecular structure of complexes **1** and **2** are built from isolated hetero-dinuclear molecules of $[(\text{DMSO})_2\text{NiLZn}(\text{NCS})_2]$ (For complex **1**, $L = L^1$ and for complex **2**, $L = L^2$), where nickel(II) is hexa-coordinated and zinc(II) is tetra-coordinated. H_2L^1 and H_2L^2 are two potential hexadentate compartmental Schiff bases

with inner N_2O_2 and outer O_4 compartments with nickel(II) occupying the inner N_2O_2 cavity and zinc(II) occupying the outer O_4 cavity. The nickel(II) centre, [Ni(1) for complex **1** and Ni(2) for complex **2**], has a pseudo-octahedral geometry, where two imine nitrogen atoms, N(1) and N(2), and two phenoxo oxygen atoms, O(1) and O(2), of the deprotonated di-Schiff base constitute the equatorial plane. The deviation of all the coordinating atoms, O(1), O(2), N(1) and N(2), in the basal plane from the mean plane passing through them are 0.100(2), $-0.100(2)$, $-0.083(3)$ and 0.084(3) Å for complex **1** and $-0.031(3)$, 0.031(3), 0.026(3) and $-0.026(3)$ Å for complex **2** respectively. The deviation of Ni(1) from the same plane is $-0.0006(5)$ Å for complex **1** and 0.0020(5) Å for complex **2** respectively. In the axial positions, the nickel(II) center is coordinated by two oxygen atoms from two DMSO molecules furnishing the distorted octahedral coordination sphere around nickel(II). The phenoxo oxygen atoms of the Schiff base are also coordinated to the zinc(II) centre, Zn(1). The bridging angles, Ni(1)–O(2)–Zn(1) and Ni(1)–O(1)–Zn(1), are 101.11(10)° and 100.36(9)° in complex **1** and 103.2(1)° and 100.8(1)° in complex **2** respectively. The dihedral angle between the Ni(1)O(1)O(2) and Zn(1)O(1)O(2) planes are 4.12° in complex **1** and 7.47° in complex **2**, indicating the Ni(1)O(1)O(2)Zn(1) core almost planar. The potential donor methoxy oxygen atoms, O(1) and O(2), of the compartmental Schiff bases remain essentially pendant and therefore the potential hexadentate Schiff bases behave as tetradentate ones in both complexes. Two nitrogen atoms, N(3) and N(4), from two thiocyanates coordinate zinc(II) to complete its distorted tetrahedral geometry in each complex. The intra-dimer nickel(II) \cdots zinc(II) distance is 3.1154(5) Å in complex **1** and 3.1410(6) Å in complex **2**.

Complex **1** shows significant C–H $\cdots\pi$ interactions. The hydrogen atom, H(23A), attached to carbon atom, C(23), is involved in an inter-molecular C–H $\cdots\pi$ interaction with a symmetry related $(2-x, -y, 1-z)$ phenyl ring [C(2)–C(3)–C(4)–C(5)–C(6)–C(7)] to form a supra-molecular dimer as shown in Fig. 3. Similarly, the hydrogen atom, H(25A), attached to carbon atom, C(25), is involved in inter-molecular C–H $\cdots\pi$ interaction with the symmetry related $(2-x, 1-y, 1-z)$ phenyl ring [C(13)–C(14)–C(15)–C(16)–C(17)–C(18)] to form another supra-molecular dimer as shown in Fig. 4. Again, inter-molecular C–H $\cdots\pi$ interaction is also observed between the hydrogen atom, H(47A) and the symmetry

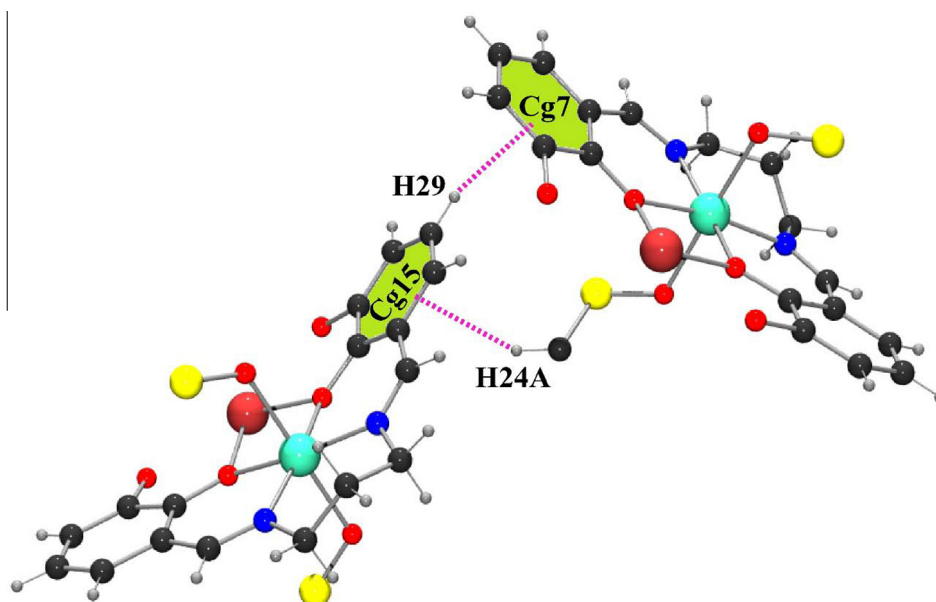


Fig. 6. Inter-molecular C–H $\cdots\pi$ interactions in complex **1** with selective atom numbering scheme. Only relevant atoms are shown in the figure.

related $(3-x, 1-y, 2-z)$ phenyl ring [C(27)–C(28)–C(29)–C(30)–C(31)–C(32)] (Fig. 5). Complex **1** also shows two intra-molecular C–H $\cdots\pi$ interactions which are confined between two different subunits of the complex having different symmetries. The hydrogen atom, H(24A), attached to carbon atom, C(24) and the hydrogen atom, H(29), attached to carbon atom C(29), is involved in intra-molecular C–H $\cdots\pi$ interactions with symmetry related $(3-x, 1-y, 2-z)$ phenyl ring [C(27)–C(28)–C(29)–C(30)–C(31)–C(32)] and $(2-x, 1-y, 1-z)$ phenyl ring [C(2)–C(3)–C(4)–C(5)–C(6)–C(7)] respectively. All these interactions are shown in Fig. 6. The details of the geometric features of the C–H $\cdots\pi$ interactions are given in Table 4.

Complex **2** shows only one inter-molecular C–H $\cdots\pi$ interaction. The hydrogen atom, H(22A), attached to carbon atom C(22), is involved in C–H $\cdots\pi$ interaction with a symmetry related $(1-x, 1-y, -z)$ phenyl ring [C(15)–C(16)–C(17)–C(18)–C(19)–C(20)] to form a supra-molecular dimer (Fig. 7). The details of the geometric features of the C–H $\cdots\pi$ interactions are given in Table 4.

3.3. Spectral and magnetic properties

Strong and sharp bands around 1626 cm^{-1} due to azomethine (C=N) groups have been routinely noticed in the IR spectra for both complexes [44]. Sharp bands in the IR spectra of complexes **1** and **2** at 2074 cm^{-1} and 2088 cm^{-1} respectively indicate the presence of thiocyanate [45].

Electronic spectra of both complexes in DMSO display absorption bands around 580 nm and 990 nm. These bands may be assigned as ${}^3T_{1g}(F) \leftarrow {}^3A_{2g}(F)$ and ${}^3T_{2g}(F) \leftarrow {}^3A_{2g}(F)$ respectively [46,47]. The higher energy d-d band, ${}^3T_{1g}(P) \leftarrow {}^3A_{2g}(F)$, cannot be observed as it is obscured by a strong charge transfer transition ($\sim 350\text{ nm}$) in each case [46,47].

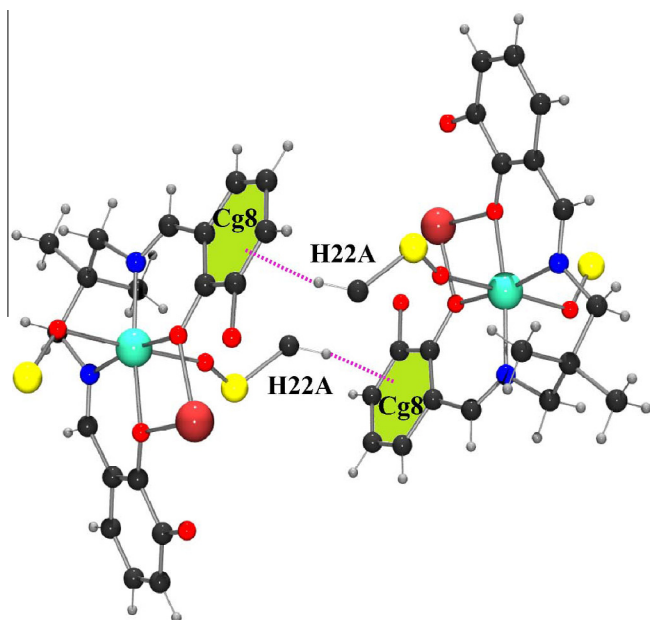


Fig. 7. Perspective view of the supra-molecular dimer formed by inter-molecular C–H $\cdots\pi$ interactions in complex **2** with selective atom numbering scheme. Only relevant atoms are shown in the figure.

Table 5
Photophysical data for complexes **1** and **2**.

Complex	Absorption (nm)	Emission (nm)
1	280	329
2	280	329

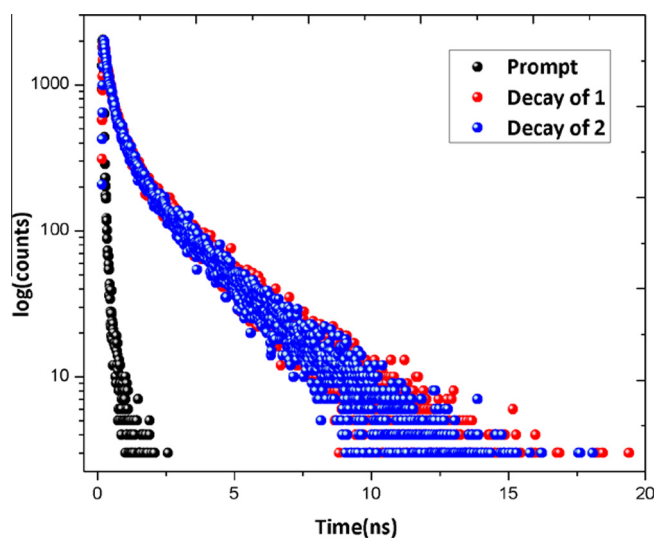


Fig. 8. Time dependent photoluminescence decay profile of complexes **1** and **2**.

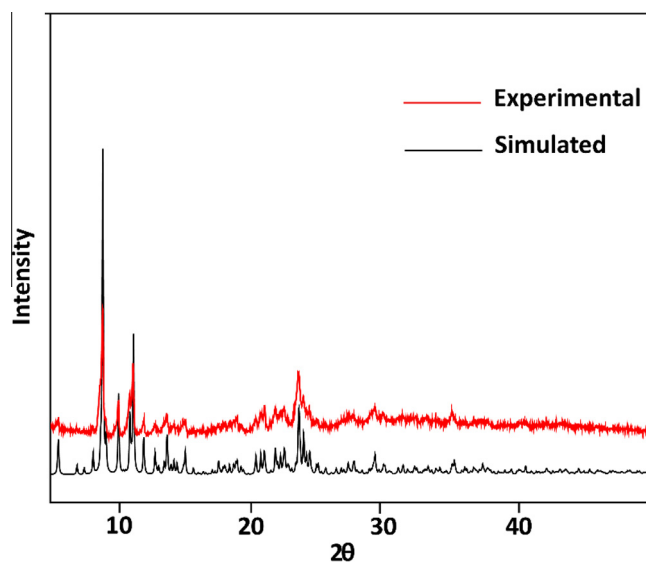


Fig. 9. Experimental and simulated PXRD patterns of complex **1** confirming purity of the bulk material.

Both complexes exhibit fluorescence in DMSO medium. The fluorescence data are listed in Table 5 (without solvent correction). These are assigned as intra-ligand (π – π^*) fluorescence [48]. The mean lifetimes (Γ_{avg}) of the excited states are 4 ns (for **1**) and 5 ns (for **2**) at room temperature. The lifetime decay profile of complexes is shown in Fig. 8.

The effective magnetic moments ($\sim 3.1\text{ BM}$) of both complexes clearly confirmed the presence of two unpaired electrons ($S = 1$) in a pseudo-octahedral environment, in agreement with high-spin configuration $t_{2g}^5e_g^2$, as was also observed in similar systems [46,47].

3.4. PXRD

The experimental PXRD patterns of the bulk products are in good agreement with the simulated XRD patterns from single crystal X-ray diffraction results, indicating consistency of the bulk sample. The simulated patterns of the complexes were calculated from the single crystal structural data using the CCDC Mercury

software. As a representative example the experimental and simulated PXRD patterns of complex **1** is shown in Fig. 9.

3.5. Hirshfeld surfaces

The Hirshfeld surfaces of the two complexes, mapped over d_{norm} (range of -0.1 to 1.5 Å), shape index and curviedness, are illustrated in Fig. 10. The surfaces are shown as transparent to allow visualization of the molecular moiety around which they are calculated. The dominant interaction between $\text{O}\cdots\text{H}/\text{H}\cdots\text{O}$ atoms can be seen in the Hirshfeld surfaces as red spots on the d_{norm} surface in Fig. 10. Other visible spots in the Hirshfeld surfaces correspond to $\text{C}\cdots\text{H}$ and $\text{H}\cdots\text{H}$ contacts. The small extent of area and light color on the surface indicates weaker and longer contact other than hydrogen bonds. The intermolecular interactions appear as distinct spikes in the 2D fingerprint plot (Fig. 11). Complementary regions are visible in the fingerprint plots where one molecule acts as donor ($d_e < d_i$) and the other as an acceptor ($d_e > d_i$). The fingerprint

plots can be decomposed to highlight particular atoms pair close contacts. This decomposition enables separation of contributions from different interaction types, which overlap in the full fingerprint. The proportions of $\text{O}\cdots\text{H}/\text{H}\cdots\text{O}$ interactions comprise 5.1% and 2.9% of the Hirshfeld surfaces for complexes **1** and **2**, respectively. This $\text{O}\cdots\text{H}/\text{H}\cdots\text{O}$ interaction also appears as two distinct spikes in the 2D fingerprint plots (Fig. 11). The lower spike corresponding to the donor spike represents the $\text{O}\cdots\text{H}$ interactions ($d_i = 1.36$, $d_e = 1.0$ Å in **1** and $d_i = 1.5$, $d_e = 1.18$ Å in **2**, respectively) and the upper spike being an acceptor spike represents the $\text{H}\cdots\text{O}$ interactions ($d_i = 1.0$, $d_e = 1.36$ Å in **1** and $d_i = 1.18$, $d_e = 1.5$ Å in **2**, respectively) in the fingerprint plot (Fig. 11). Similarly the proportion of $\text{C}\cdots\text{H}/\text{H}\cdots\text{C}$ interactions comprises 20.5% and 17.8% of the Hirshfeld surfaces for complexes **1** and **2**, respectively. This $\text{C}\cdots\text{H}/\text{H}\cdots\text{C}$ interaction also appears as two distinct spikes in the 2D fingerprint plots (Fig. 11). The lower spike corresponding to the donor spike represents the $\text{C}\cdots\text{H}$ interactions ($d_i = 1.59$, $d_e = 1.1$ Å in **1** and $d_i = 1.56$, $d_e = 1.0$ Å in **2**, respectively) and the

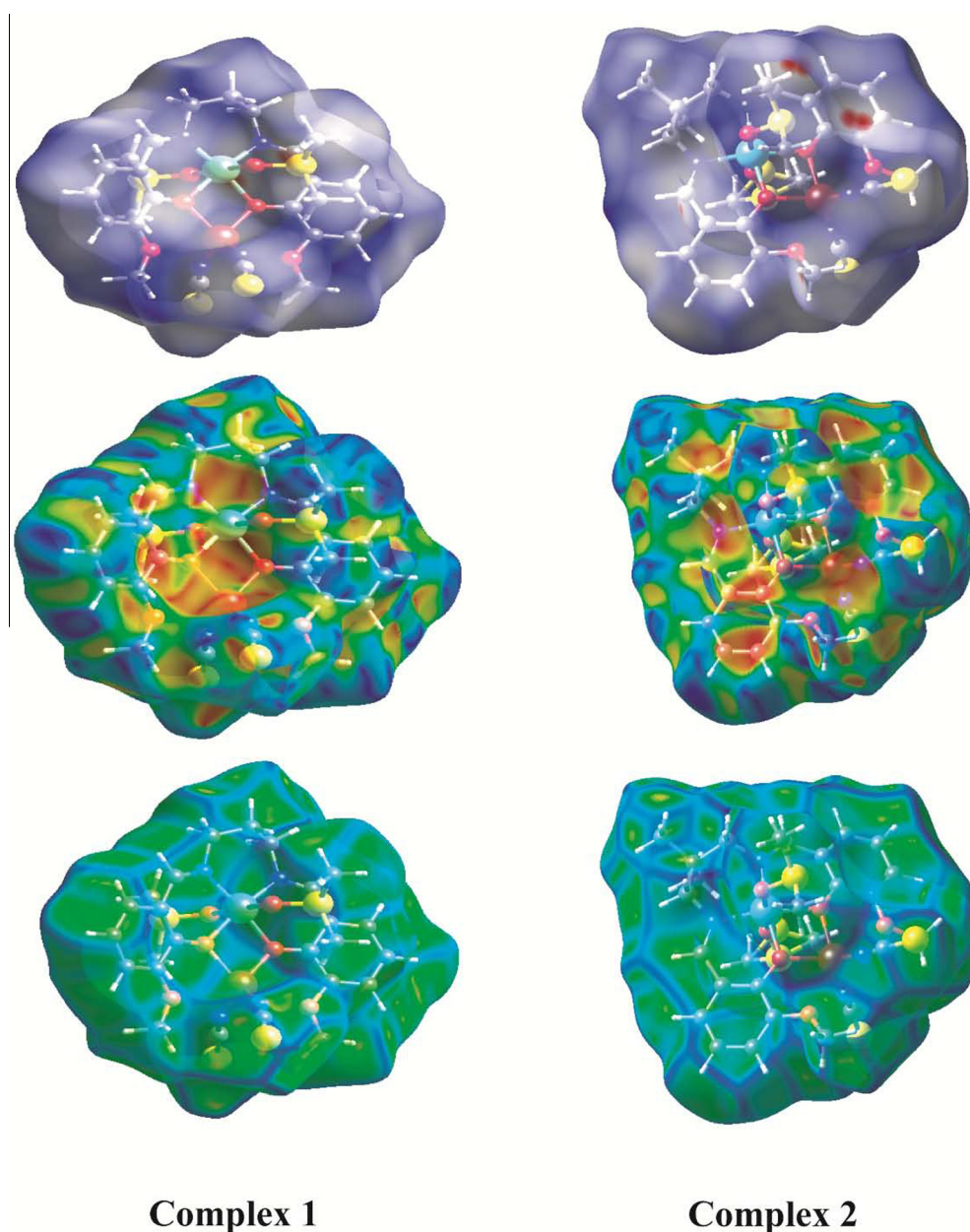


Fig. 10. Hirshfeld surfaces mapped with d_{norm} (top), shape index (middle) and curviedness (bottom) of complexes **1** and **2**.

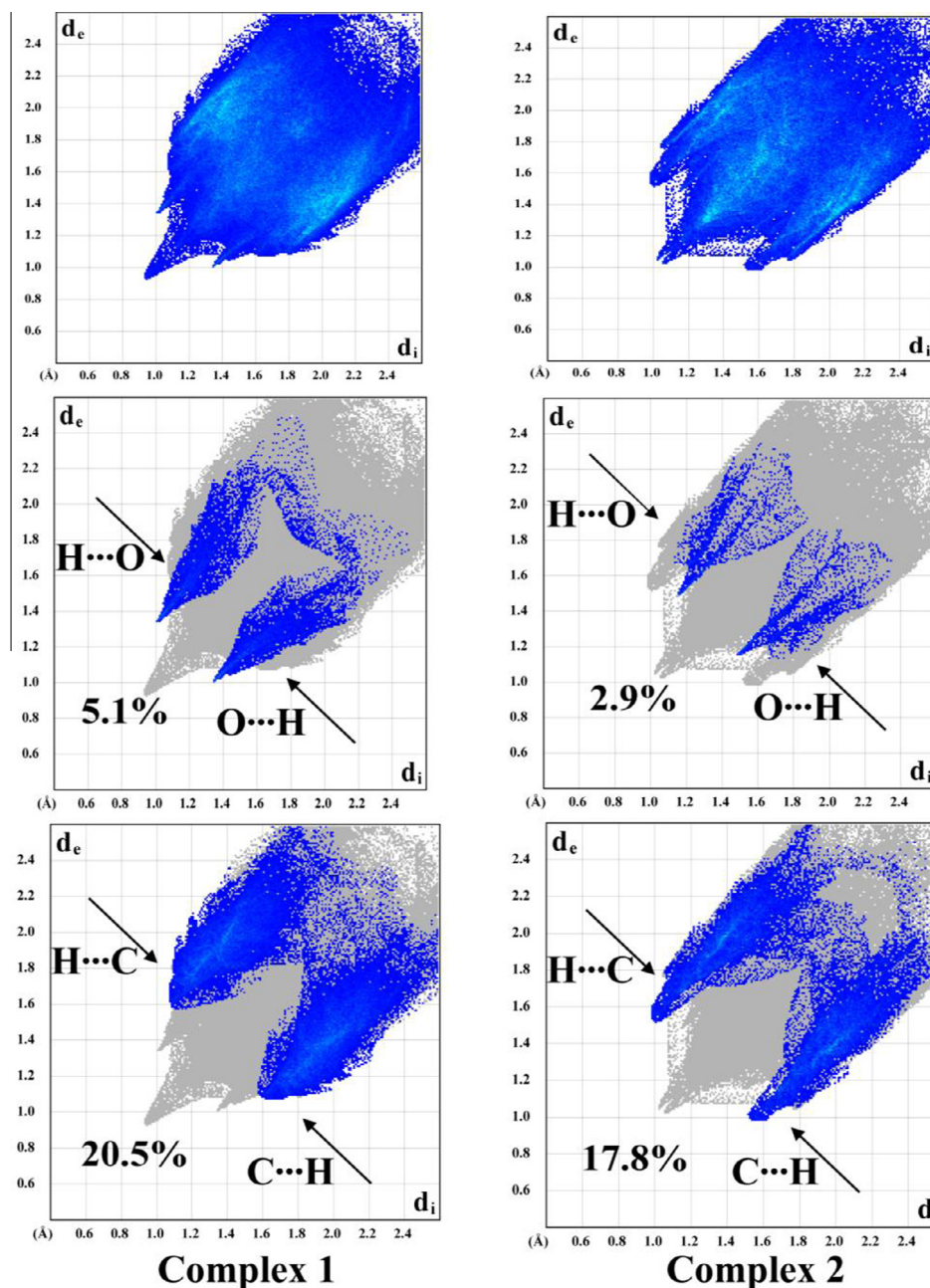


Fig. 11. Fingerprint plot: Full (top), resolved into $H\cdots O/O\cdots H$ (middle) and $H\cdots C/C\cdots H$ (bottom) contacts contributed to the total Hirshfeld Surface area of complexes 1 and 2.

upper spike being an acceptor spike represents the $H\cdots C$ interactions ($d_i = 1.1$, $d_e = 1.59$ Å in **1** and $d_i = 1.0$, $d_e = 1.56$ Å in **2**, respectively) in the fingerprint plot (Fig. 11).

4. Concluding remarks

The tandem synthesis and characterization of two iso-structural complexes $[(DMSO)_2NiL^1Zn(NCS)_2]$ (**1**) and $[(DMSO)_2NiL^2Zn(NCS)_2]$ (**2**) have been described in the present paper. It has been presented that the reaction of nickel(II) thiocyanate tetrahydrate and zinc(II) with potential hexadentate N_2O_4 donor compartmental Schiff bases can afford hetero-dinuclear complexes with nickel(II) sitting in the inner N_2O_2 compartment and zinc(II) sitting in the outer O_4 compartment. Use of only nickel(II) produces mononuclear species containing nickel(II) in the inner N_2O_2 cavity. These mononuclear

nickel(II) complexes could not be converted into the hetero-dinuclear nickel(II)/zinc(II) complexes on reacting with zinc(II) and thiocyanate. The beauty of the present work, therefore, lies in the discovery of one pot synthesis of these hetero-dinuclear complexes. Given the novel role of zinc(II) in the field of electronic and opto-electronic research, the present findings may provide insight and serve as a prototype for preparing other such complexes. Work is in progress to get better yield of the reaction and to synthesize other photo-luminescent hetero-dinuclear complexes.

Acknowledgments

A.B. thanks the UGC, India, for awarding a Senior Research Fellowship. Crystallographic data were collected at the DST-FIST, India, funded by Single Crystal Diffractometer Facility at the Department of Chemistry, Jadavpur University.

Appendix A. Supplementary data

CCDC 1444181 and 1444182 contain the supplementary crystallographic data for **1** and **2**, respectively. These data can be obtained free of charge via <http://www.ccdc.cam.ac.uk/conts/retrieving.html>, or from the Cambridge Crystallographic Data Centre, 12 Union Road, Cambridge CB2 1EZ, UK; fax: (+44) 1223-336-033; or e-mail: deposit@ccdc.cam.ac.uk. Supplementary data associated with this article can be found, in the online version, at <http://dx.doi.org/10.1016/j.poly.2016.03.026>.

References

- [1] C.-L. Hu, J.-G. Mao, *Coord. Chem. Rev.* 288 (2015) 1.
- [2] G.N.D. Francesco, A. Gaillard, I. Ghiviriga, K.A. Abboud, L.J. Murray, *Inorg. Chem.* 53 (2014) 4647.
- [3] S. Chattopadhyay, M.G.B. Drew, C. Diaz, A. Ghosh, *Dalton Trans.* (2007) 2492.
- [4] S. Halder, A. Mukherjee, K. Ghosh, S. Dey, M. Nandi, P. Roy, *J. Mol. Struct.* 1101 (2015) 1.
- [5] W.L. Ping, J.S. Bo, Z.W. Feng, L.Y. Qi, Y. Gui, *Chin. Sci. Bull.* 58 (2013) 2733.
- [6] D. Sadhukhan, A. Ray, G. Pilet, C. Rizzoli, G.M. Rosair, C.J. Gomez-Garcia, S. Signorella, S. Bell, S. Mitra, *Inorg. Chem.* 50 (2011) 8326.
- [7] S. Bag, P.K. Bhaumik, S. Jana, M. Das, P. Bhowmik, S. Chattopadhyay, *Polyhedron* 65 (2013) 229.
- [8] J. Yuan, W.-B. Shi, H.-Z. Kou, *Transition Met. Chem.* 40 (2015) 807.
- [9] G. Dyer, D.W. Meek, *Inorg. Chem.* 6 (1967) 149.
- [10] M. Das, S. Chatterjee, S. Chattopadhyay, *Polyhedron* 68 (2014) 205.
- [11] M. Palmieri, G. Malgieri, L. Russo, I. Baglivo, S. Esposito, F. Netti, A.D. Gatto, I. de Paola, L. Zaccaro, P.V. Pedone, C. Isernia, D. Milardi, R. Fattorusso, *J. Am. Chem. Soc.* 135 (2013) 5220.
- [12] D. Li, X. Tian, G. Hu, Q. Zhang, P. Wang, P. Sun, H. Zhou, X. Meng, J. Yang, J. Wu, B. Jin, S. Zhang, X. Tao, Y. Tian, *Inorg. Chem.* 50 (2011) 7997.
- [13] S. Shit, A. Sasmal, P. Dhal, C. Rizzoli, S. Mitra, *J. Mol. Struct.* 1108 (2016) 475.
- [14] H. Wang, X.-Y. Zhang, C.-F. Bi, Y.-H. Fan, X.-M. Meng, *Transition Met. Chem.* 40 (2015) 769.
- [15] S. Ghosh, A. Ghosh, *Inorg. Chim. Acta* 442 (2016) 64.
- [16] M. Sakamoto, K. Manseki, H. Okawa, *Coord. Chem. Rev.* 219–221 (2001) 379.
- [17] M. Das, S. Chatterjee, S. Chattopadhyay, *Inorg. Chem. Commun.* 14 (2011) 1337.
- [18] A. Biswas, M. Ghosh, P. Lemoine, S. Sarkar, S. Hazra, S. Mohanta, *Eur. J. Inorg. Chem.* (2010) 3125.
- [19] P. Bhowmik, S. Jana, P.P. Jana, K. Harms, S. Chattopadhyay, *Inorg. Chem. Commun.* 18 (2012) 50.
- [20] P. Bhowmik, S. Jana, S. Chattopadhyay, *Polyhedron* 44 (2012) 11.
- [21] P. Bhowmik, S. Chatterjee, S. Chattopadhyay, *Polyhedron* 63 (2013) 214.
- [22] P. Bhowmik, S. Jana, P.P. Jana, K. Harms, S. Chattopadhyay, *Inorg. Chim. Acta* 390 (2012) 53.
- [23] S. Bhattacharyya, A. Jana, S. Mohanta, *Polyhedron* 62 (2013) 234.
- [24] S. Thakurta, C. Rizzoli, R.J. Butcher, C.J.G. Garcia, E. Garrirba, S. Mitra, *Inorg. Chim. Acta* 363 (2010) 1395.
- [25] M. Sarwar, A.M. Madalan, C. Tiseanu, G. Novitchi, C. Maxim, G. Marinescu, D. Luneau, M. Andruh, *New J. Chem.* 37 (2013) 2280.
- [26] A. Jana, S. Majumder, L. Carrella, M. Nayak, T. Weyhermueller, S. Dutta, D. Schollmeyer, E. Rentschler, R. Koner, S. Mohanta, *Inorg. Chem.* 49 (2010) 9012.
- [27] L. Zhang, X. Li, Y. Zhang, *J. Mol. Struct.* 1103 (2016) 56.
- [28] K. Singh, A. Kumar, R. Srivastava, P.S. Kadyan, M.N. Kamalasanan, I. Singh, *Opt. Mater.* 34 (2011) 221.
- [29] K.P. Sarma, R.K. Poddar, *Transition Met. Chem.* 9 (1984) 135.
- [30] G.M. Sheldrick, *Acta Crystallogr., Sect. A* 64 (2008) 112.
- [31] G.M. Sheldrick, *SHELXS-97* and *SHELXL-97*: Program for Structure Solution, University of Göttingen, Institute für Anorganische Chemie der Universität, Göttingen, Germany, 1997.
- [32] G.M. Sheldrick, *SADABS*: Software for Empirical Absorption Correction, University of Göttingen, Institute für Anorganische Chemie der Universität, Göttingen, Germany, 1999–2003.
- [33] M.A. Spackman, D. Jayatilaka, *CrystEngComm* 11 (2009) 19.
- [34] F.L. Hirshfeld, *Theor. Chim. Acta* 44 (1977) 129.
- [35] H.F. Clausen, M.S. Chevallier, M.A. Spackman, B.B. Iversen, *New J. Chem.* 34 (2010) 193.
- [36] A.L. Rohl, M. Moret, W. Kaminsky, K. Claborn, J.J. McKinnon, B. Kahr, *Cryst. Growth Des.* 8 (2008) 4517.
- [37] A. Parkin, G. Barr, W. Dong, C.J. Gilmore, D. Jayatilaka, J.J. McKinnon, M.A. Spackman, C.C. Wilson, *CrystEngComm* 9 (2007) 648.
- [38] M.A. Spackman, J.J. McKinnon, *CrystEngComm* 4 (2002) 378.
- [39] S.K. Wolff, D.J. Grimwood, J.J. McKinnon, D. Jayatilaka, M.A. Spackman, *Crystal Explorer 2.0*, University of Western Australia, Perth, Australia, 2007. <<http://hirshfeldsurfacenet.blogspot.com>>.
- [40] J.J. McKinnon, M.A. Spackman, A.S. Mitchell, *Acta Crystallogr., Sect. B* 60 (2004) 627.
- [41] A. Datta, B. Machura, J.-H. Huang, S.-C. Sheu, *Acta Crystallogr., Sect. E* 69 (2013) m399.
- [42] A. Elmalia, C.T. Zeyrek, Y. Elermana, Z. Naturforsch. 59b (2004) 228–232.
- [43] J.-P. Costes, B. Donnadiou, R. Gheorghe, G. Novitchi, J.-P. Tuchagues, L. Vendier, *Eur. J. Inorg. Chem.* (2008) 5235.
- [44] P. Bhowmik, H.P. Nayek, M. Corbella, N. Aliaga-Alcalde, S. Chattopadhyay, *Dalton Trans.* 40 (2011) 7916.
- [45] S. Roy, A. Dey, P.P. Ray, J. Ortega-Castro, A. Frontera, S. Chattopadhyay, *Chem. Commun.* 51 (2015) 12974.
- [46] A. Bhattacharyya, P.K. Bhaumik, M. Das, A. Bauzá, P.P. Jana, K. Harms, A. Frontera, S. Chattopadhyay, *Polyhedron* 101 (2015) 257.
- [47] S. Chattopadhyay, M.G.B. Drew, A. Ghosh, *Polyhedron* 26 (2007) 3513.
- [48] A. Bhattacharyya, K. Harms, S. Chattopadhyay, *Inorg. Chem. Commun.* 48 (2014) 12.